

# Compact Dual-Band Monopole Antennas with Fractal-Based Half- and Quarter-Circular Folded Loops for WiMAX and WLAN Applications

Dhirgham K. Naji\*

*The Department of Electronic and Communications Engineering  
College of Engineering, Al-Nahrain University, Baghdad, Iraq*

**ABSTRACT:** In this paper, two new types of dual-band antennas are presented: a coplanar waveguide (CPW)-fed fractal monopole antenna (FMA) and an asymmetric coplanar strip (ACS)-fed fractal half-monopole antenna (FHMA). These antennas are designed to operate in two distinct bands suitable for 3.5/5.5 GHz WiMAX and 5.2/5.8 GHz WLAN applications. Both antennas possess the property of self-similarity by employing half- and quarter-circular folded loops, respectively, which represent the antennas' radiating elements. A design procedure based on a conventional circular patch antenna (CPA) is performed, with evolution steps leading to the achievement of the proposed two antennas with the above-mentioned features. To validate the design concept, two simulator programs (CST MWS and HFSS) were used to extract the simulated results regarding reflection coefficient  $s_{11}$ , gain, efficiency, and radiation patterns. According to the agreement between the CST and HFSS simulated results, prototypes of the FMA and FHMA are fabricated on an FR4 substrate with a dielectric constant of 4.4, a height of 0.8 mm, and overall sizes of only  $26 \times 20 \text{ mm}^2$  and  $12 \times 19 \text{ mm}^2$ , representing nearly 73% and 40% reduction in size, respectively, compared with the size of  $26 \times 33 \text{ mm}^2$  for the CPA. The simulated and measured  $s_{11}$  results are in good agreement, illustrating the two antennas operating over the desired bands ( $s_{11} \leq -10 \text{ dB}$ ): 3.5-/5.5-GHz (3.40–3.69 and 5.25–5.85 GHz) WiMAX and 5.2-/5.8-GHz (5.15–5.35 and 5.72–5.85 GHz) WLAN. Furthermore, the peak realized gain values are greater than 2 dBi, efficiency exceeding 90%, and nearly omnidirectional radiation at both bands. Based on the achieved results and antennas' compactness, they can be highly recommended for the use in WLAN and WiMAX applications.

## 1. INTRODUCTION

In the rapidly evolving landscape of wireless communication, there is a growing need for compact antenna designs, especially for WiMAX (Worldwide Interoperability for Microwave Access) and WLAN (Wireless Local Area Network) applications. As these technologies continue to progress, the requirement for antennas that function well across various frequency bands while keeping a compact size is becoming more essential [1]. Multiband antennas with outstanding radiation properties and a wide impedance bandwidth are essential for meeting the demands of WLAN and WiMAX applications across various frequency ranges, including 2.4–2.484 GHz, 5.15–5.825 GHz, as well as 3.4–3.69 GHz, and 5.25–5.85 GHz [2]. The feeding structure is a crucial factor when designing compact antennas. Commonly used feeding methods in printed antenna designs are a microstrip (MS) and coplanar waveguide (CPW) transmission line. The CPW-fed technique offers several benefits compared to the MS feeding structure, including single-layer metallization, minimal dispersion, the capability to control characteristic impedance, and reduced radiation loss [3]. Recently, asymmetrical coplanar strips (ACSs), which feature a single lateral ground plane as opposed to the dual lateral grounds found in CPW lines

have gained popularity among antenna engineers. This design approach with an ACS structure allows for compact antenna (around 40% reduction in size in comparison with its counterpart CPW structures) while maintaining principles similar to those of coplanar transmission lines [4].

To design an antenna capable of supporting multiband and broadband operations, several microstrip antenna designs have been proposed for effectively covering the 3.5-/5.5-GHz WiMAX and 5.2-/5.8-GHz WLAN. These designs primarily utilized monopole patch antennas and excited by either CPW [5–12] or ACS feeding configuration [13–17]. In [5], a CPW-fed dual-band slotted-ring monopole antenna with circular fractal elements is reported. By inserting specific slot configurations in the radiator, this design provides dual operating bands of 3.15 to 3.75 GHz and 5.02 to 7.58 GHz. In [6], a  $22 \times 22 \text{ mm}^2$  size pentagonal ring fractal antenna, excited by a CPW feedline, is presented to achieve two frequency bands (3.12–3.82 GHz and 5.16–5.83 GHz) with resonances around 3.4 and 5.5 GHz, respectively. A fractal monopole antenna in the shape of a 9-point star, featuring a band-notched design is described in [7]. Incorporating a pair of L-shaped slots into its ground planes allows it to effectively operate in two specific frequency ranges: from 3.05 to 3.84 GHz and from 5.15 to 5.825 GHz. However, it has a large size of  $30 \times 45 \text{ mm}^2$ . A semi-circular microstrip antenna that uses a tapered ground

\* Corresponding author: Dhirgham Kamal Naji (dhirgham.kamal.1@nahrainuniv.edu.iq).

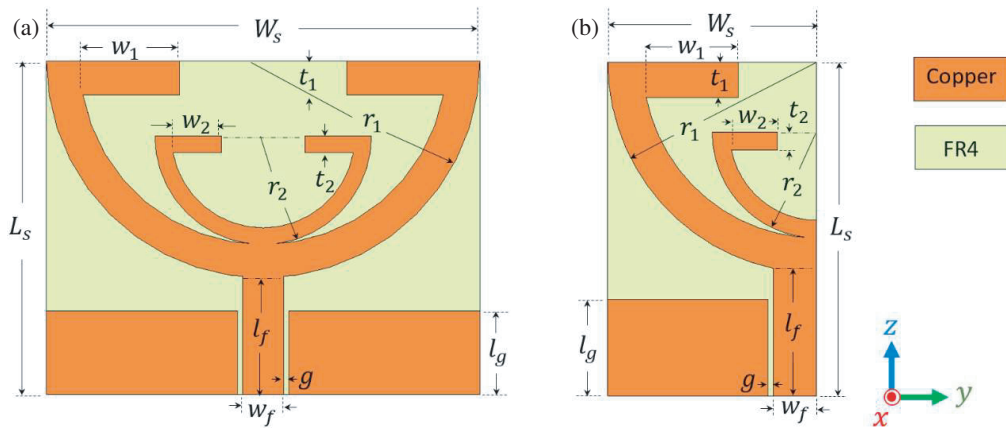


**FIGURE 1.** Geometry of the proposed fractal antennas. (a) Front side of the CPW-fed FMA. (b) Front side of the ACS-fed FHMA.

plane and a folded U-shaped slot within the patch is presented in [8]. With a  $17 \text{ mm} \times 18 \text{ mm}$  dimension, it operates within two working bands of 3.4 to 3.7 GHz and 5.725 to 5.875 GHz.

In [9], a CPW-fed metamaterial-inspired wideband antenna was reported. The antenna achieved a wide bandwidth ranging from 3.06 GHz to 5.89 GHz, which makes it suitable for 3.3/3.5/5.5 GHz WiMAX and 5.2/5.8 GHz WLAN applications. To obtain the desired dual-band operation, a circularly-slotted antenna with two sets of unequally inverted L-shaped strips linked to the ground plane is reported in [10]. In [11], a fractal antenna was developed using the third iteration of the pentagonal Sierpinski gasket island, intended for applications in 3.5 GHz WiMAX and 5.2 GHz WLAN. A rupee-shaped patch of a CPW-fed antenna with dimensions of  $17.5 \times 17.5 \times 1.6 \text{ mm}^3$  was reported in [12]. A dual-band characteristic of 2.92–3.7 GHz and 4.6–6.0 GHz is achieved by the designed antenna by attaching an additional horizontal L-shaped strip.

An ACS-fed L-profile double-band monopole antenna design for 3.5 GHz WiMAX and 5.8 GHz WLAN functions was presented in [13]. It was developed from its counterpart CPW-fed antenna in three evolution stages with area reduction of around 44%. In [14], a hook-shaped monopole antenna fed by ACS structure was proposed. To achieve two independently controlled frequency bands centered at 3.5 and 5.2 GHz, the antenna used a quarter-wavelength strip with a C-shaped half-wavelength loop strip. Another ACS-fed dual-band planar antenna with an area of  $21 \times 15.35 \text{ mm}^2$  was designed in [15]. By using defected ground and defected microstrip structures, the antenna operates at two distinct frequencies of 3.5 GHz and 5.5 GHz, which correspond to WiMAX and WLAN bands, respectively. In [16], a compact monopole antenna with an F-shape was designed for the use in 3.5/5.5 GHz WiMAX and 5.8 GHz WLAN applications. The F-shaped ACS-fed antenna includes a U-shaped open-ended slot that has been precisely tuned to create a band notch at 4.5 GHz. This slot enables the antenna to support two frequency passband ranges from 3.3 to 3.8 GHz and from 5.5 to 6.5 GHz. Despite the reported antennas being designed to effectively meet the required WiMAX and WLAN frequency bands, some of them have either a large

size, a complicated structure, or a narrowed upper frequency band, making them unsuitable for portable communication devices.

It can be concluded from the preceding discussion that there is still a demand for dual-band antennas with compact dimensions, wide bandwidth, acceptable radiation characteristics, and simplified geometrical structure. Therefore, a compact-size CPW-fed fractal monopole antenna (FMA) and an ACS-fed fractal half monopole antenna (FHMA) are proposed in this paper. The CPW and ACS antennas fabricated on a low cost 0.8-mm thick FR-4 substrate with small footprint areas of  $26 \times 20 \text{ mm}^2$  and  $12 \times 19 \text{ mm}^2$ , respectively. The CST MWS and HFSS simulation softwares were used, respectively, to predict and validate the performance of antennas including the reflection coefficient  $s_{11}$ , gain, efficiency, and radiation patterns. The structures of both antennas and their design methods are discussed in details in Section 2. The simulated and measured results of the fabricated antennas along with discussions are presented in Section 3. The conclusion is provided in Section 4.

## 2. THE PROPOSED DESIGNED ANTENNAS AND STRUCTURES

This section presents the configuration of the proposed antennas, with a detailed explanation of their design evolution. Initially, a conventional circular patch antenna (CPA) which serves as the reference antenna is designed, from which the proposed designed antennas are developed after passing through four evolutionary steps. Then, a parametric study for main geometric antenna parameters is conducted, and the primary concept of antenna operation is demonstrated by investigating their surface current distributions at resonance frequencies.

### 2.1. Antenna Configuration

The geometries of the proposed antennas, FMA and its counterpart FHMA, are shown in Figs. 1(a) and 1(b), respectively. The monopole of FMA (FHMA) comprises a second-order fractal-based half- (quarter)-circular folded loop with dimension parameters: radii  $r_1, r_2 (= 0.5r_1)$ , width of the folded arm  $w_1$ ,

$w_2 (= 0.5w_1)$  and thickness  $t_1, t_2 (= 0.5t_1)$ . These  $50 \Omega$  CPW and ACS feeding lines are connected to the monopole of the FMA and FHMA, respectively, with length  $l_f$ , width  $w_f$ , and a gap  $g$  between the signal strip and the coplanar ground of length  $l_g$ . The two antennas were printed on the front side of an FR4 substrate with an overall size of ( $W_s \times L_s$ ), thickness ( $h_s = 0.8$  mm), dielectric constant ( $\epsilon_r = 4.4$ ), and loss tangent ( $\tan \delta = 0.02$ ) and devoid of metallization on the back side of the substrate. The modeled SMA connector was considered in the 3D full-wave electromagnetic (EM) solvers, CST MWS and HFSS, for correctly modeling the proposed antennas. Table 1 summarizes the optimized dimensions of the CPW-fed FMA and ACS-fed FHMA.

**TABLE 1.** Optimized dimensions of the proposed antennas, CPW-fed FMA and ACS-fed FHMA.

Parameter	Value (mm)	
	CPW-fed FMA	ACS-fed FHMA
$L_s$	20	19
$W_s$	26	12
$h_s$	0.8	0.8
$w_f$	2.5	2.5
$l_f$	7	7
$l_g$	5	5.5
$g$	0.3	0.3
$r_1$	13	12
$r_2$	6.5	6
$w_1$	6	5.5
$w_2$	3	2.75
$t_1$	2	2
$t_2$	1	1

## 2.2. Design Evolution Process

A detailed design evolution process is discussed here to show how a reference antenna CPA was initially designed with specified parameters (resonance frequency  $f_r$ , substrate height  $h_s$ , and dielectric constant  $\epsilon_r$ ). Then, subsequently four design steps (Fig. 2) are applied to CPA until the proposed antennas achieve the desired operating dual frequency bands with compact sizes. Fig. 3 shows the effect of structural modifications on the antennas' reflection coefficient ( $s_{11}$ ). Tables 2 and 3 summarize the performance parameters of the CPW and ACS antennas, respectively, in terms of  $-10$  dB impedance bandwidth in the two bands (Band 1 and Band 2), resonance frequencies ( $f_{r1}$  and  $f_{r2}$ ), and reflection coefficients at resonance frequencies ( $s_{11}|_{f_{r1}}$  and  $s_{11}|_{f_{r2}}$ ). These design steps are discussed as follows.

### 2.2.1. Initial Design Step

In this initial step, a conventional CPA, as shown in Fig. 4 (inscribed inside the plot of  $s_{11}$ ), is used as a reference antenna and designed for operating at  $f_r = 3.3$  GHz, the lower frequency in the 3.5-GHz WiMAX band. Then, radius  $r_1$  of the circular

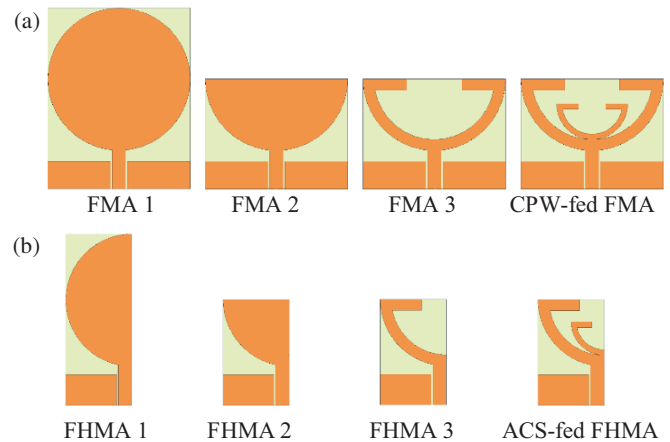


**FIGURE 2.** Design evolution of proposed antennas: (a) CPW-fed FMA and (b) ACS-fed FHMA.

patch is calculated by (1) [17].

$$(f_r)_{mn0} = \frac{\chi'_{mn} v_0}{2\pi r_1 \sqrt{\epsilon_r}} \quad (1)$$

where  $v_0$  is the speed of light in free space;  $m$  and  $n$  denote mode numbers; and  $\chi'_{mn}$  is a coefficient that determines the order of the resonant frequencies for the  $TM_{mn0}$  modes. Substitute in (1) the following values for the dominant  $TM_{110}$  mode:  $m = n = 1$ ,  $\chi'_{11} = 1.8421$ ,  $\epsilon_r = 4.3$ , and  $(f_r)_{110} = 3.3$  GHz, resulting in  $r_1$  of 13 mm. Then, on the front side of the FR substrate of size ( $W_s \times L_s$ ), a circular patch of the CPA with  $r_1 = 13$  mm is connected to a  $50 \Omega$  microstrip line of length  $l_f$  and width  $w_f$ . A full metallization ground is printed on the back side of the substrate.

A CST MWS is used to model and analyze the reference antenna. Table 4 lists the optimized dimensions, and Fig. 4 shows the simulated reflection coefficient  $s_{11}$  result. As observed, four resonance frequencies (3.3, 5.5, 6.5, and 7.5 GHz) are excited from this antenna, which represent the first four resonant frequencies ( $f_r)_{mn0}$  (3.27, 5.42, 6.80, and 7.46) corresponding to the  $TM_{mn0}$  modes calculated by (1). Table 5 summarizes these frequencies obtained from the calculated and simulated results, which are very close to each other. This reference antenna is considered a backbone for designing the proposed antennas.

### 2.2.2. Design Step 1

In this first step, the CPA that was designed previously is modified by replacing its microstrip transmission line structure with the CPW feeding technique, and FMA1 is obtained with  $r_1 = 13$  mm with an overall size of  $W_s \times L_s (= 26 \times 33 \text{ mm}^2)$  as shown in Fig. 2(a). Also, the full ground printed on the backside of the FR4 substrate of the reference antenna is removed, and instead, a pair of partial ground planes with length  $l_g = 5$  mm is printed at a gap  $g = 0.3$  mm from the CPW central strip. Then, the right half part of FMA1 is removed, and its CPW transmission line is replaced by the ACS line, resulting in FHMA1 having a size of  $(12 \times 31 \text{ mm}^2)$  with reducing  $r_1$  to 12 mm, as noticed in Fig. 2(b). The width

**TABLE 2.** Performance parameters for the four different steps of evolved CPW-fed FMA.

Design step	Band 1			Band 2		
	BW1 (GHz)	$f_{r1}$ (GHz)	$s_{11 f_{r1}}$ (dB)	BW2 (GHz)	$f_{r2}$ (GHz)	$s_{11 f_{r2}}$ (dB)
<b>FMA1</b>	2.6–5.8	3.1, 4.8	−18.4, −28.1	N/A	N/A	N/A
<b>FMA2</b>	3.4–7.7	4.0	−17.2	N/A	N/A	N/A
<b>FMA3</b>	3.3–4.0	3.6	−13.3	N/A	N/A	N/A
<b>Prop. FMA</b>	<b>3.3–3.8</b>	<b>3.5</b>	<b>−14.0</b>	<b>4.6–5.9</b>	<b>5.0</b>	<b>−23.4</b>

**TABLE 3.** Performance parameters for the four different steps of evolved ACS-fed FHMA.

Design step	Band 1			Band 2		
	BW1 (GHz)	$f_{r1}$ (GHz)	$s_{11 f_{r1}}$ (dB)	BW2 (GHz)	$f_{r2}$ (GHz)	$s_{11 f_{r2}}$ (dB)
<b>FHMA1</b>	2.6–3.6	3.0	−24.4	4.9–7.1	5.9	−25.3
<b>FHMA2</b>	3.6–6.1	4.3, 5.3	−17.7, −19.6	N/A	N/A	N/A
<b>FHMA3</b>	3.2–3.8	3.5	−13.0	6.7–> 8.0	7.54	−25.9
<b>Prop. FHMA</b>	<b>3.3–3.8</b>	<b>3.5</b>	<b>−14.1</b>	<b>5.1–6.2</b>	<b>5.5</b>	<b>−15.4</b>

Abbreviation: N/A, not available

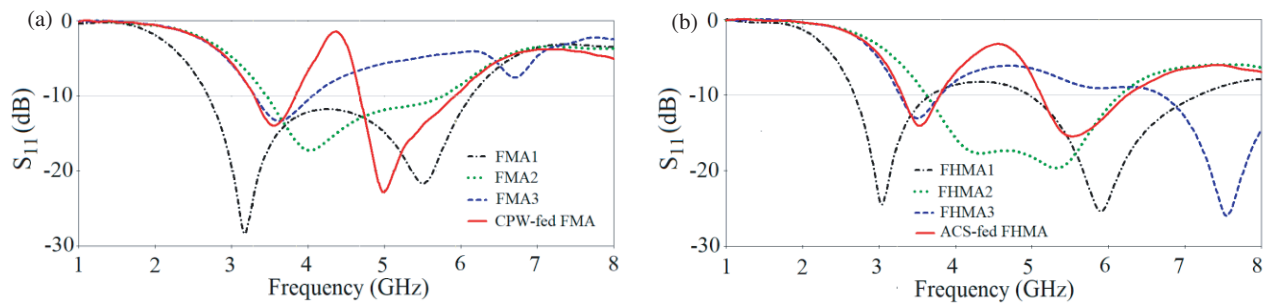


**FIGURE 3.** Effect of structural modifications shown in Fig. 2 on the antenna reflection coefficient  $s_{11}$ : (a) CPW-fed FMA, (b) ACS-fed FHMA.

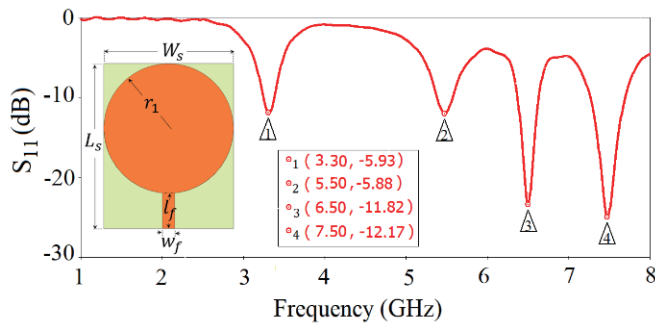


**FIGURE 4.** The simulated reflection coefficient  $s_{11}$  characteristic for the conventional microstrip-fed circular patch antenna (CPA).

**TABLE 4.** Dimensions of the conventional microstrip-fed circular patch antenna.

Parameter	$L_s$	$W_s$	$h_s$	$r_1$	$w_f$	$l_f$
<b>Value (mm)</b>	33	26	0.8	13	1.6	7

$w_f = 2.5$  mm and length  $l_f = 7.0$  mm of the central strip besides  $g = 0.3$  mm are used as main dimension parameters for CPW and ACS structures to ensure a  $50 \Omega$  characteristic impedance

**TABLE 5.** The first four resonance frequencies of the conventional CPA.

Mode (mn)	$\chi_{mn}$	$(f_r)_{mn0}$ (GHz)	
		By simulation	By calculation
11	1.8412	3.3	3.27
21	3.0542	5.5	5.42
01	3.8318	6.5	6.80
31	4.2012	7.5	7.46

properly matched with their input impedances. The aforementioned CPW and ACS main parameters besides partial ground length are kept unaltered for the remaining design steps. As observed in Fig. 3, Tables 2 and 3, FMA1 radiates only the greater  $-10$  dB matching bandwidth (Band 1) from 2.62 to 5.8 GHz for  $s_{11} \leq -10$  dB with two resonance frequencies 3.13 and 4.83 GHz with minimum reflection coefficients of  $-18.47$  and  $-28.12$  dB, respectively (Fig. 3(a), dash-dotted black curve), whereas FHMA1 operates at two bands (Fig. 2(b), dash-dotted black curve): Band 1 (2.68–3.67 GHz)

with  $f_{r1} = 3.04$  GHz and  $s_{11}|_{f_{r1}} = -24.48$  dB; Band 2 (4.96–7.18 GHz) with  $f_{r2} = 5.9$  GHz and  $s_{11}|_{f_{r2}} = -25.36$  dB. Since both antennas fail to cover the desired bands: Band 1 (3.3–3.8 GHz) and Band 2 (5.15–5.85 GHz), they must be developed to have compact sizes and satisfy these bands.

### 2.2.3. Design Step 2

In this design step, a half-circular patch is used as a radiating element for FMA2 by cutting the upper-half circle of FMA1 as shown in Fig. 2(a). Thus, the size of FMA2 ( $W_s \times L_s$ ) is ( $= 26 \times 20$  mm<sup>2</sup>), where  $W_s$  remains unchanged, and  $L_s$  becomes 20 mm, which is lower than  $L_s = 33$  mm for FMA1 by the value of  $r_1 = 13$  mm. Therefore, a gain in size reduction of nearly 40% is achieved by this process. Similarly, FHMA2 with a quarter-circular patch is evolved from FHMA1 by removing its upper quarter circle of radius  $r_1 = 12$  mm, as portrayed in Fig. 2(b). Hence, the overall size of FHMA2 is ( $12 \times 19$  mm<sup>2</sup>), resulting in around 38.7% size reduction compared with the size of FHMA1. One can notice from Fig. 3(a) (Fig. 3(b)) the dotted green curve, and Table 2 (Table 3) that FMA2 (FHMA2) covers a wide bandwidth ranging from 3.45 (3.62) to 7.76 GHz (6.15 GHz) with  $f_r = 4.02$  GHz ( $f_r = 4.32$  and 5.32 GHz). Also, more modifications are required to make the proposed antennas, CPW-fed FMA and its counterpart ACS-fed FHMA, to verify the aforementioned desired bands while keeping their sizes fixed at  $26 \times 20$  mm<sup>2</sup> and  $12 \times 19$  mm<sup>2</sup>, respectively.

### 2.2.4. Design Step 3

This part of the design process produces FMA3 (FHMA3), which comprises a first-order fractal folded half- (quarter)-circular loop strip with a radius  $r_1$  of 13 mm (12 mm), thickness  $t_1 = 2$  mm, and folded-arm width  $w_1$  of 6.0 mm (5.5 mm), developed from its counterpart half- (quarter)-circular patch of FMA2 (FHMA2), as shown in Fig. 2(a) (Fig. 2(b)). 50  $\Omega$  CPW and ACS transmission lines with same dimensions described in the previous two design steps are used here to feed these antennas, FMA3 and FHMA3, respectively. As shown in Fig. 3(a) and Fig. 3(b) (blue dashed-curve), FMA3 radiates only one resonance frequency of 3.62 GHz within Band 1 (3.30–4.06 GHz) while FHMA3 covers two bands: Band 1 (3.27–3.80 GHz) with  $f_r = 3.5$  GHz and Band 2 (6.7 — greater than 8 GHz) with  $f_r$  of 7.54 GHz. It can also be seen from Tables 2 and 3 that the desired lower band (3.3–3.8 GHz) is nearly covered by both the antennas, but the higher band (5.15–5.85 GHz) is not. So, more modifications must be applied to both antennas to properly produce the dedicated lower and higher frequency bands.

### 2.2.5. Design Step 4

In this final design step, the CPW-fed FMA and ACS-fed FHMA, as shown in Figs. 2(a) and 2(b), are obtained as the proposed antennas by adding resonant structures represented by the second-order fractal half- and quarter-circular loops to FMA3 and FHMA3, respectively. The second-order fractal half- (quarter)-circular loop represents a copied version of its

counterpart first-order loop with a fractal scale factor  $k = 0.5$ , radius  $r_2$  of 6.5 mm (6.0 mm), thickness  $t_2 = 1$  mm, and folded-arm width  $w_2$  of 3.0 mm (2.75 mm). As observed in Figs. 3(a) and 3(b), red solid curves, the addition of a new fractal resonator into the CPW and ACS antennas results in a downshift of their upper band (Band 2) to the specified band (5.15–5.85 GHz) without altering the lower band (Band 1).

In summary, it is demonstrated that while maintaining antenna compactness, the proper inclusion of extra resonant structures to the antenna would efficiently provide unprecedented degrees of freedom for controlling the higher frequency band with a slight effect on the lower band. Thus, this feature can be more attractive for designing multiband antennas with compact sizes and simple structures.

## 2.3. Parametric Study

The key geometric parameters affecting the resonance frequencies  $f_{r1}$  and  $f_{r2}$  besides the notch frequency  $f_{\text{notch}}$  are the width  $w_1$  of the folded arm, thickness  $t_1$  of the first-order fractal circular loop, ground length  $l_g$ , and fractal scale factor  $k$ . Indeed, the width  $w_2$  of the folded arm and thickness  $t_2$  of the second-order fractal circular loop are also studied implicitly since  $w_2 = 0.5w_1$  and  $t_2 = 0.5t_1$ . In this study, while one parameter is under analysis, the others preserve their optimized dimensions.

### 2.3.1. Varying Folded Arm Width ' $w_1$ '

The influences of varying folded arm width  $w_1$  on reflection coefficient spectra  $s_{11}$  and the three frequencies  $f_{r1}$ ,  $f_{r2}$ , and  $f_{\text{notch}}$  for both antennas, FMA and FHMA, are shown in Fig. 5(a) and Fig. 6(a), respectively. It can be observed that when  $w_1$  is permitted to increase within the defined intervals, all three frequencies for both antennas largely decrease ( $\downarrow\downarrow$ ), as illustrated in Table 6. However, the magnitude of  $s_{11}$  at these frequencies remains nearly unchanged for FMA, while it is significantly affected for FHMA with the variation of  $w_1$ . As stated earlier, as  $w_1$  is varied the corresponding  $w_2$  also varies since  $w_2$  is related to  $w_1$  by the relation  $w_2 = 0.5w_1$ . This study concludes that any variation in the dimension of  $w_1$  for both antennas would strongly affect the two resonance modes in the two bands as well as the correspondent notch frequency between the bands.

### 2.3.2. Varying Thickness of the Circular Loop ' $t_1$ '

Figures 5(b) and 6(b) depict the effect of variation in the thickness ' $t_1$ ' on the  $s_{11}$  alongside resonance frequencies and notch frequency for the CPW- and ACS-fed antennas, respectively. A closer inspection into Figs. 5(b), 6(b), and Table 6 indicates that  $f_{r1}$  slightly increases ( $\uparrow$ ), and  $f_{\text{notch}}$  slightly decreases ( $\downarrow$ ) whereas  $f_{r2}$  largely increases ( $\uparrow\uparrow$ ) for both antennas as  $t_1$  increases. On the other hand, the magnitudes of  $s_{11}$  at  $f_{r1}$ ,  $f_{\text{notch}}$ , and  $f_{r2}$  are increased, unchanged, and decreased, respectively, as  $t_1$  increases for both antennas. Additionally, the first lower frequency  $f_{l1}$  in Band 1 and the second higher frequency  $f_{h2}$  in Band 2 for the antennas are nearly unaffected by varying  $t_1$  from 1.2 to 2.8 mm. Thus, the dimensions of thickness ' $t_1$ ' and

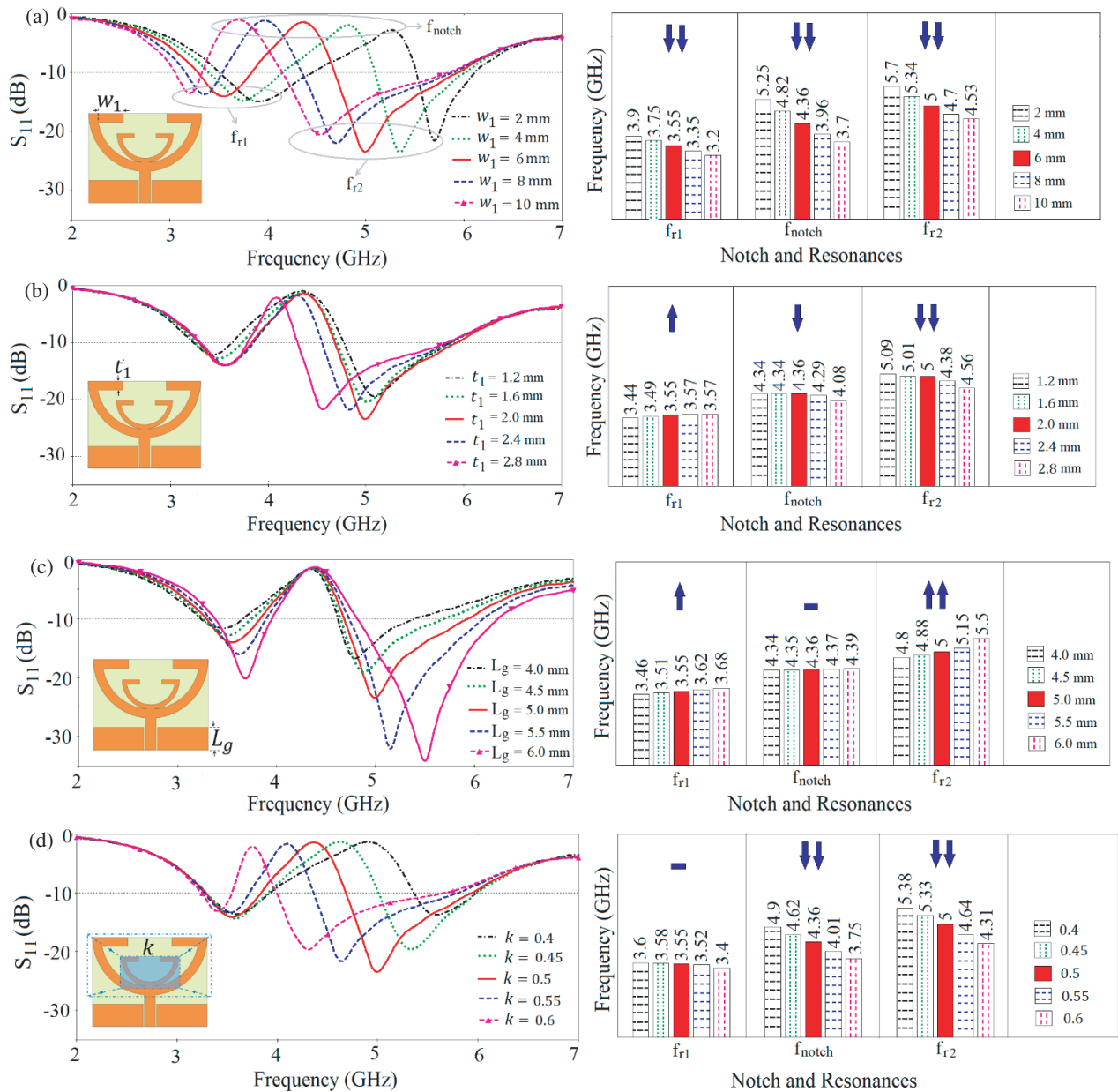


**FIGURE 5.** Impact of sweeping (a)  $w_1$ , (b)  $t_1$ , (c)  $l_g$ , and (d)  $k$  on the reflection coefficient alongside notch frequency and resonances of the CPW-fed FMA.

accordingly ‘ $t_2$ ’ can be adjusted to accurately specify the resonance frequencies within the desired  $-10$  dB antenna matching bandwidths.

**2.3.3. Varying Ground Length ‘ $l_g$ ’**

Figures 5(c) and 6(c) elucidate the impact of variation in the ground length  $l_g$  on the FMA and FHMA impedance bandwidths, respectively. As noted from these figures and Table 6, the notch frequency  $f_{notch}$  for the two antennas is almost unchanged (-).  $f_{r1}$  slightly increases ( $\uparrow$ ), and  $f_{r2}$  strongly increases ( $\uparrow\uparrow$ ) when  $l_g$  is allowed to vary within the specified ranges. Furthermore, the value of  $s_{11}$  at  $f_{r1}$  is increased and at  $f_{notch}$  is unaltered for both antennas with increase (decrease) in  $|s_{11}|$  at  $f_{r2}$  for FMA (FHMA) when  $l_g$  is increased. On the

other hand, the higher frequencies,  $f_{h1}$  in Band 1 and  $f_{h2}$  in Band 2, are largely influenced by varying  $l_g$ .

Thus, the dimension  $l_g$  can be considered a key geometric parameter to be used properly for fine-tuning the resonance frequencies within the lower and upper antenna impedance bands while maintaining the notched band unaltered.

**2.3.4. Varying Fractal Scale Factor ‘ $k$ ’**

The effect of the fractal scale factor  $k$  on the reflection coefficient of the CPW and ACS antennas is depicted in Figs. 5(d) and 6(d), respectively. It can be observed in these two figures and Table 6 that by increasing  $k$  from 0.4 to 0.6 with a step size of 0.05, the lower band for both antennas is slightly affected, especially the lower frequency  $f_{l1}$  whereas  $f_{r1}$  is approximately

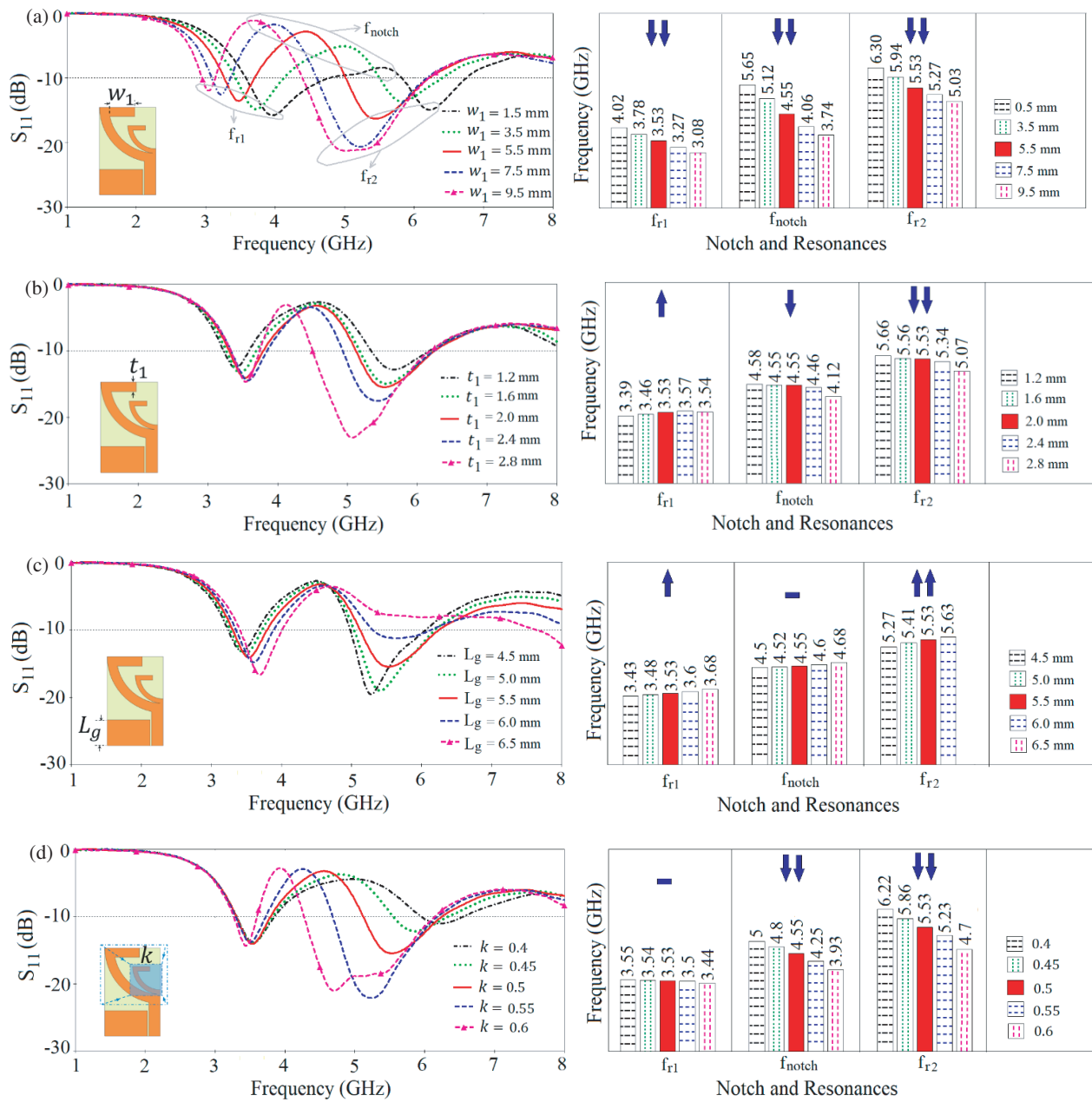


**FIGURE 6.** Impact of sweeping (a)  $w_1$ , (b)  $t_1$ , (c)  $l_g$ , and (d)  $k$  on the reflection coefficient alongside notch frequency and resonances of the ACS-fed FHMA.

**TABLE 6.** Influence of geometrical parameters of the antennas on resonance frequencies and notch frequency. The mark (\*) denotes that the variation ranges of  $w_1$  and  $l_g$  within brackets belong to ACS-fed FHMA.

Parameter	$w_1$	$t_1$	$l_g$	$k$	
Variation range (mm)	2.0–10 (1.5–9.5)*	1.2–2.8	4.0–6.0 (4.5–6.5)*	0.4–0.6	
Step size (mm)	2	0.4	0.5	0.05	
CPW-fed FMA	$f_{r1}$ (GHz)	3.90–3.20 (↓)	3.44–3.57 (↑)	3.46–3.68 (↑)	3.60–3.40 (-)
	$f_{r2}$ (GHz)	5.70–4.53 (↓)	4.34–4.08 (↓)	4.80–5.50 (↑)	5.38–4.31 (↓)
	$f_{notch}$ (GHz)	5.25–3.7 (↓)	5.09–4.56 (↓)	4.34–4.39 (-)	4.90–3.75 (↓)
ACS-fed FHMA	$f_{r1}$ (GHz)	4.02–3.08 (↓)	3.39–3.54 (↑)	3.34–3.68 (↑)	3.55–3.44 (-)
	$f_{r2}$ (GHz)	6.30–5.03 (↓)	5.66–5.07 (↓)	5.27–5.63 (↑)	6.22 – –4.70 (↓)
	$f_{notch}$ (GHz)	5.65–3.74 (↓)	4.58–4.12 (↓)	4.50–4.68 (-)	5.00–3.93 (↓)

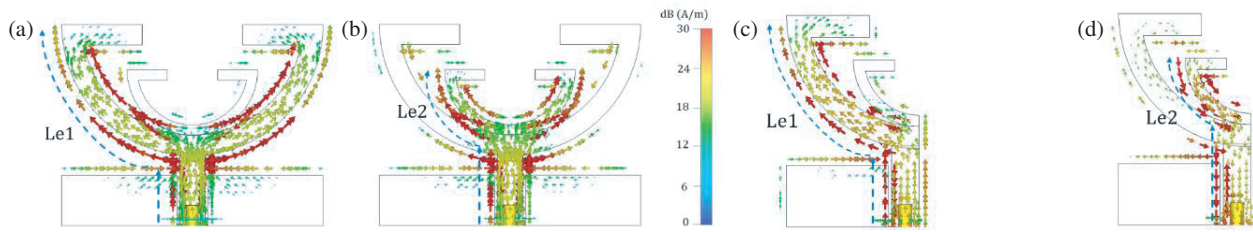


**FIGURE 7.** The surface current distribution of: CPW-fed FMA (a) at 3.5 GHz, (b) at 5.5 GHz; ACS-fed FHMA at (c) at 3.5 GHz; (d) at 5.5 GHz.

**TABLE 7.** The geometric parameters and resonance frequencies used for calculating the effective current paths,  $L_{e1}$  and  $L_{e2}$ .

Parameter	Value	
	CPW-fed FMA	ACS-fed FHMA
$r_1$	13 mm	12 mm
$r_2$	6.5 mm	6.0 mm
$f_{r1}$	3.55 GHz	3.53 GHz
$f_{r2}$	5.00 GHz	5.53 GHz

unaffected (–), and the notched and upper bands characterized by  $f_{\text{notch}}$  and  $f_{r2}$ , respectively, are largely decreased ( $\downarrow\downarrow$ ). Additionally, the magnitude of  $s_{11}$  for both antennas remains nearly unchanged at  $f_{r1}$  and  $f_{\text{notch}}$ , while an increase in  $s_{11}$  is observed at  $f_{r2}$  as  $k$  increases. Therefore, the fractal scale factor  $k$  plays a significant role in efficiently shifting the higher frequency range to the desired band without any effect on the lower band and its resonance frequency.

#### 2.4. Surface Current Distribution

To investigate the proposed antennas’ principal operation further and highlight the role of the two resonance modes in radiation, the simulated surface current distribution at their resonance frequencies is presented in Fig. 7. It can be observed in Fig. 7(a) (Fig. 7(b)) that more current distribution at 3.55 GHz (5.0 GHz) is mostly concentrated along the effective path  $L_{e1}$  ( $L_{e2}$ ) constituting the outer sides of the CPW stripline and the large (small) half-circular loop.

Similarly, as observed in Fig. 7(c) (Fig. 7(d)), the surface current distribution at 3.53 GHz (5.53 GHz) mainly flows along the path  $L_{e1}$  ( $L_{e2}$ ) which comprises the outer edges of the ACS stripline and the large (small) quarter-circular loop. Thus, all fractal elements of the proposed antennas have contributed to exciting the magnetic current, confirming that these elements represent the main radiating antenna structures responsible for creating the resonance frequencies.

To get more physical insights into the dual-band operation in CPW (ACS) feed antenna, the optimized dimensions and, calculated electrical lengths  $L_{e1}$  and  $L_{e2}$  in terms of guided half-wavelengths  $0.5\lambda_{g1}$  and  $0.5\lambda_{g2}$  for resonant frequencies of 3.55 (3.53) and 5.0 GHz (5.53 GHz), are presented to validate the design concept. As shown in Fig. 7, the optimized dimensions of  $L_{e1}$  and  $L_{e2}$  can be calculated as

$$L_{e1} = c_1 + l_f \quad (2a)$$

**TABLE 8.** The calculated effective current path and the corresponding half-wave guided wavelength for each resonance frequency.

Parameter	Value (mm)	
	CPW-fed FMA	ACS-fed FHMA
$L_{e1}$	27.40	25.80
$L_{e2}$	19.20	16.40
$0.5\lambda_{d1}$	25.95	26.10
$0.5\lambda_{d2}$	18.45	16.65

$$L_{e2} = c_2 + l_f \quad (2b)$$

where  $l_f$  is the length of the stripline;  $c_1$  and  $c_2$  denote the lengths of the quarter arc for the large and small circles with radii  $r_1$  and  $r_2$ , respectively, given by  $c_1 = \pi r_1 / 2$  and  $c_2 = \pi r_2 / 2$ . The guided wavelengths  $\lambda_{g1}$  and  $\lambda_{g2}$  are given by

$$\lambda_{g1} = v_0 / f_{r1} \sqrt{\epsilon_e} \quad (3a)$$

$$\lambda_{g2} = v_0 / f_{r2} \sqrt{\epsilon_e} \quad (3b)$$

where  $f_{r1}$  and  $f_{r2}$  are the first and second resonance frequencies, respectively, and  $\epsilon_e$  stands for the effective dielectric constant of the substrate, which is given by

$$\epsilon_e = (\epsilon_r + 1) / 2 \quad (4)$$

By substituting  $l_f = 7$  mm and  $\epsilon_r = 4.3$  in (2) and (3), and using the values of the radii  $r_1$ ,  $r_2$  and resonance frequencies  $f_{r1}$ ,  $f_{r2}$  for the CPW and ACS antennas from Table 7, one can calculate the effective current path and the corresponding half-guided wavelength for each resonance frequency, which are listed in Table 8.

As noticed in Table 8, the effective electrical length and half-guided wavelength at each resonance frequency are highly close, that is  $L_e \cong 0.5\lambda_d$  for the CPW- and ACS-fed antennas.

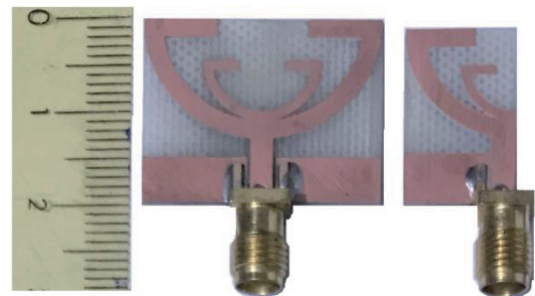


**FIGURE 8.** Photograph of the fabricated antennas. Left: CPW-fed monopole antenna. Right: ACS-fed half monopole antenna.

Hence, the two passbands and notched frequencies can be easily controlled by adjusting the dimension parameters of the fractal resonator elements.

### 3. RESULTS AND DISCUSSIONS

To validate the proposed design, prototypes of the proposed antennas were fabricated, and the measured reflection coefficient  $s_{11}$  is presented. Then, CST MWS and HFSS simulation results in terms of  $s_{11}$ , far-field radiation patterns in  $E$ - and  $H$ -planes at resonance frequencies, and peak realized gain and efficiency versus several frequencies of the desired bands are reported.

Figure 8 shows the fabricated antennas, and their reflection coefficient characteristics are measured using an Agilent Vector Network Analyzer (VNA: E5071C). The measured and simulated impedance bandwidths against frequency for the CPW- and ACS-fed antennas are depicted in Figs. 9(a) and 9(b), respectively. Table 9 summarizes the performance parameters:  $-10$  dB impedance bandwidth (IBW), resonance frequency ( $f_r$ ), notch frequency  $f_{notch}$  of the measured results, and CST MWS and HFSS simulated results.

As observed in Table 9, there is a good agreement between the simulated and measured results with a small discrepancy due to either the tolerance error in the fabrication process, uncertainty of the dielectric constant, or losses result-

ing from soldering the SMA connector. As noticed in Table 9, the measured  $-10$  dB IBWs for the CPW feed antenna are: Band 1: 600 MHz (3.8–3.9 GHz) with  $f_{r1} = 3.26$  GHz and Band 2: 1150 MHz (3.85–5.0 GHz) with  $f_{r2} = 4.15$  GHz with  $f_{notch} = 4.15$  GHz. Furthermore, the measured  $-10$  dB IBWs for the ACS feed antenna are: Band 1: 900 MHz (3.05–3.95 GHz) with  $f_{r1} = 3.55$  GHz and Band 2: 900 MHz (5.25–6.15 GHz) with  $f_{r2} = 5.65$  GHz with  $f_{notch} = 4.35$  GHz. These make the proposed antennas suitable for operating at the desired bands: 3.5 GHz WiMAX (3.3–3.8 GHz), 5.2/5.8 GHz WLAN, and 5.5 GHz WiMAX (5.15–5.85 GHz).

The CST and HFSS simulated 2D far-field radiation patterns for the proposed antennas in both  $E$ -plane ( $yz$ -plane) and  $H$ -plane ( $xz$ -plane), at two different passband frequencies (3.5 and 5.5 GHz), are depicted in Fig. 10. As seen in Fig. 10(a), a CPW antenna exhibits omnidirectional and nearly bidirectional radiation (dumbbell-shaped) in  $H$ -plane at 5.5 and 3.5 GHz, respectively; the radiation properties are relatively omnidirectional with a null along  $y$ -axis in the  $E$ -plane at the considered frequencies, as shown in (Fig. 10(b)). Figs. 10(c) and 10(d) portray the radiation characteristics for the ACS feed antenna in the  $xz$ -plane and  $yz$ -plane, respectively, at the two frequencies. As observed in Fig. 10(c), the radiation in the  $H$ -plane at 5.5 GHz is relatively stable and mono-directional toward the  $x$ -axis and slightly deteriorated at 3.5 GHz, and Fig. 10(d) shows that the

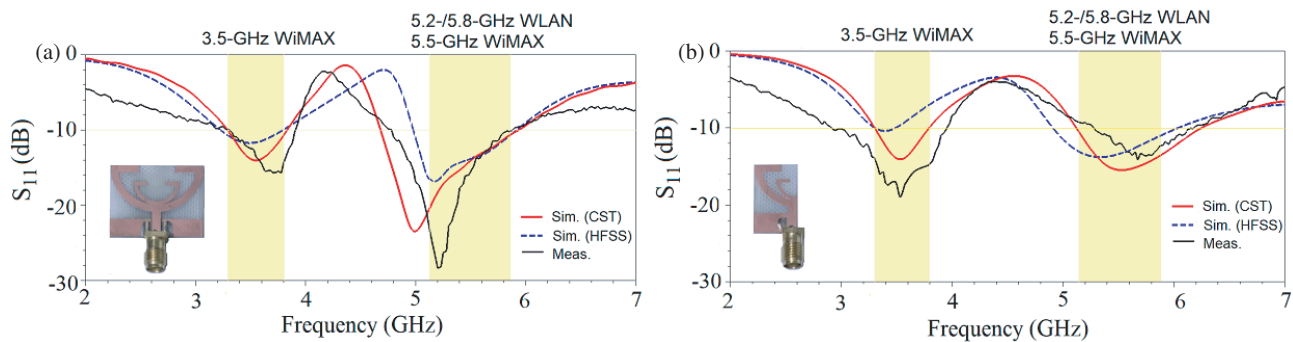
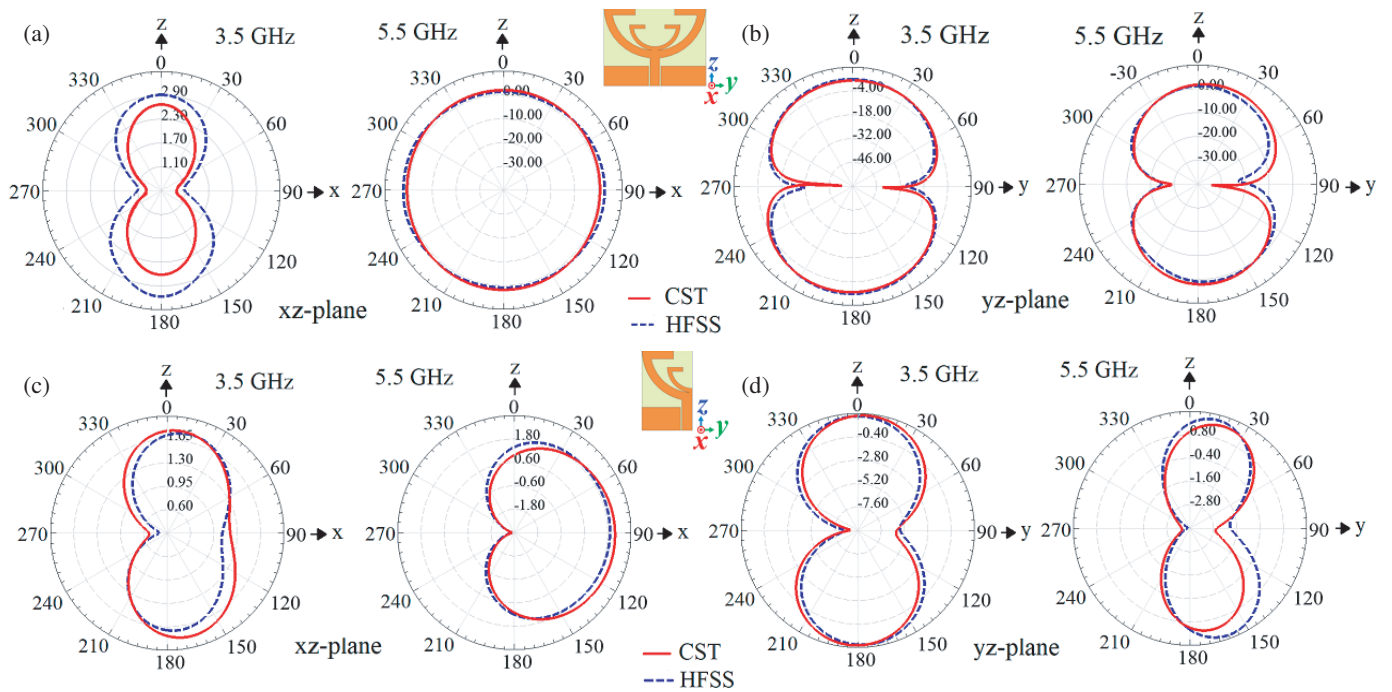


FIGURE 9. Simulated and measured return losses of proposed antennas. (a) CPW-fed FMA. (b) ACS-fed FHMA.

TABLE 9. Performance parameters:  $-10$  dB impedance bandwidth (IBW), resonance frequency ( $f_r$ ) and notch frequency  $f_{notch}$  of the measured results along with CST MWS and HFSS simulated results.

Antenna Type	Performance Parameters		CST MWS	HFSS	Measurement
CPW-fed FMA	IBW (GHz)	Band 1	3.30–3.83	3.20–3.80	3.30–3.90
		Band 2	4.68–5.93	4.96–5.95	5.00–5.85
	$f_r$ (GHz)	Band 1	3.55	2.45	3.62
		Band 2	5.00	5.18	5.20
	$f_{notch}$ (GHz)	4.38	4.75	4.15	
ACS-fed FHMA	IBW (GHz)	Band 1	3.30–3.80	3.30–3.45	3.05–3.95
		Band 2	5.12–6.25	4.90–6.00	5.25–6.15
	$f_r$ (GHz)	Band 1	3.53	3.38	3.55
		Band 2	5.53	5.30	5.65
	$f_{notch}$ (GHz)	4.57	4.40	4.35	



**FIGURE 10.** The CST and HFSS simulated 2D radiation patterns in the *H*-plane (*xz*-plane) and *E*-plane (*yz*-plane) for the proposed antenna at 3.5 and 5.5 GHz. (a) The *xz*-plane and (b) the *yz*-plane for the CPW-fed antenna. (c) The *xz*-plane and (d) the *yz*-plane for the ACS-fed antenna.

**TABLE 10.** Comparison of simulated performance parameters of the proposed antennas (peak gain and efficiency) obtained by CST MWS and HFSS simulators.

Antenna	Simulator	Band 1		Band 2	
		Peak Gain (dB)	Efficiency (%)	Peak Gain (dB)	Efficiency (%)
CPW-fed FMA	CST	2.36	93.86	1.95	94.00
	HFSS	1.82	93.44	1.58	92.04
ACS-fed FHMA	CST	2.40	97.50	1.56	98.27
	HFSS	1.86	88.05	1.34	92.06

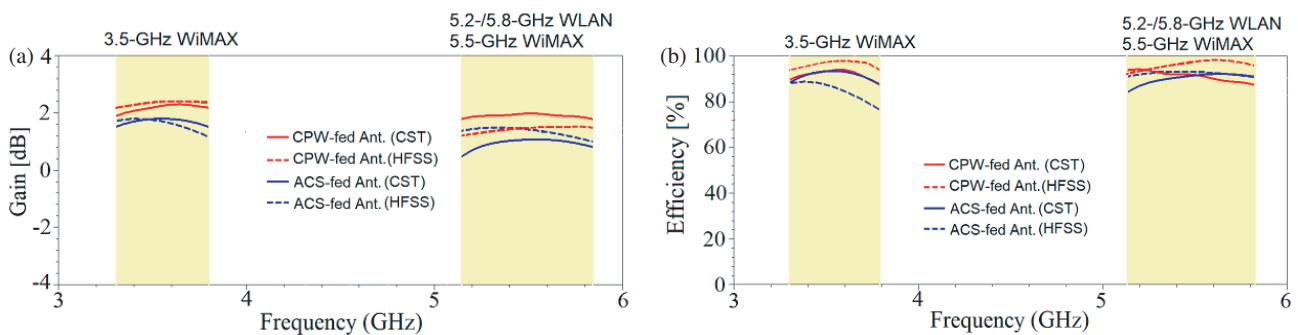


**FIGURE 11.** The CST and HFSS simulated gains and efficiencies against frequency plot for the proposed antennas. (a) Gain. (b) Efficiency.

radiation in the *E*-plane at the operating frequencies is slightly tilted and bidirectional along the *z*-axis.

The CST and HFSS simulated peak gains and efficiencies against frequency in the desired bands (3.5 GHz WiMAX) and (5.2-/5.8-GHz WLAN, 5.5-GHz WiMAX) of the proposed an-

tennas are shown in Fig. 11, and Table 10 summarizes these results.

As observed in Fig. 11(a), the CST simulated gain for the CPW antenna (ACS antenna) varies over the range 1.88 dB ~ 2.36 dB (2.16 dB ~ 2.40 dB) in the lower band and 1.78 dB ~ 2.00 dB (1.20 dB ~ 1.56 dB) in the upper band. The

**TABLE 11.** Comparison between the proposed work and some reported CPW- and ACS-fed dual-band antennas.

Ref. No.	Feeding Method	Antenna Size (mm <sup>2</sup> )	Substrate ( $\epsilon_r/h$ (mm))	-10 dB bandwidth (GHz) (WiMAX/WLAN) (3.5/5.5), (5.2/5.8)	Peak Gain (dBi)	Maximum Radiation Efficiency (%)
6	CPW	22 × 22	FR4 (4.4/1.6)	3.12–3.82 5.15–5.83	2.04 3.44	98.0 91.4
7	CPW	30 × 45	FR4 (4.4/1.6)	3.05–3.84 5.24–7.54	2.63 4.68	95.0 93.0
8	CPW	17 × 18	FR4 (4.4/0.8)	3.30–3.71 5.70–5.94	2.05 2.62	96.0 99.2
10	CPW	40 × 30	FR4 (4.4/1.6)	3.26–3.86 5.02–6.2	3.23 5.93	96.0 97.0
<b>This work</b>	<b>CPW</b>	<b>20 × 26</b>	<b>FR4 (4.4/0.8)</b>	3.30–3.90 5.00–5.85	<b>2.36</b> <b>1.95</b>	<b>9.38</b> <b>9.40</b>
13	ACS	12.5 × 20	FR4 (4.4/1.6)	3.39–3.61 5.38–7.27	1.53 3.90	89.1 92.2
14	ACS	7.9 × 20	FR4 (4.4/1.6)	2.85–3.50 4.70–6.40	2.00 2.00	72.0 72.0
15	ACS	12.35 × 20	FR4 (4.4/1.6)	3.40–3.75 5.38–5.85	2.30 3.50	N/A
16	ACS	11 × 20	FR4 (3.2/0.508)	3.30–3.80 5.50–6.50	1.80 3.50	85.0 95.0
<b>This work</b>	<b>ACS</b>	<b>12 × 19</b>	<b>FR4 (4.4/0.8)</b>	<b>3.05–3.95</b> <b>5.25–6.15</b>	<b>2.40</b> <b>1.56</b>	<b>9.75</b> <b>9.83</b>

Abbreviation: N/A, not available

maximum simulated efficiency (Fig. 11(b)) for both antennas is above 93% across the entire frequency bands of interest. Thus, this is a nearly acceptable agreement between the CST and HFSS simulation results, with a slight difference due to the different numerical techniques used in these two programs.

A comparative analysis of the proposed antennas alongside some recently reported antennas is presented in Table 11. The analysis shows that the designed CPW and ACS antennas achieve the widest bandwidth for the intended dual operating bands: 3.5/5.5-GHz WiMAX and 5.2/5.8-GHz WLAN. Additionally, the CPW and ACS antennas introduced in this work are more compact than many of the reported counterpart antennas. Moreover, the peak gain and maximum radiation efficiency of the designed antennas are high enough to be acceptable, making the prototypes good candidates for WiMAX and WLAN applications.

#### 4. CONCLUSION

In this paper, two compact dual-band CPW- and ACS-fed antennas suitable for WLAN and WiMAX applications have been designed, parametrically analyzed, and fabricated. The CPW and ACS antennas are printed on an FR-4 substrate with compact sizes of  $26 \times 20 \times 0.8 \text{ mm}^3$  and  $12 \times 19 \times 0.8 \text{ mm}^3$ , respectively. These two designed antennas are developed from a reference antenna, a circular patch antenna (CPA). Different

iterations based on a fractal technique have been made to realize dual-band CPW and ACS antennas, achieving 73% and 40% reduction in size, respectively, compared with their counterpart reference antenna. In addition to that the proposed antennas are compact in size and operate at separate frequency bands, they are characterized by a simple configuration and easy manufacture due to their planar structures. The experimental results demonstrate that the CPW- and ACS-fed antennas exhibit dual operating bands: 600 MHz (3.8–3.9 GHz) and 1150 MHz (3.85–5.0) GHz; 900 MHz (3.05–3.95 GHz) and 900 MHz (5.25–6.15 GHz), respectively. Hence, the WiMAX bands (3.5/5.5 GHz) and WLAN bands (5.2/5.8 GHz) are properly covered by the designed antennas. Additionally, these two antennas provide a gain more than 2 dBi, radiation efficiency exceeding 90%, and stable radiation patterns across the two operating frequency bands.

#### REFERENCES

- [1] Selvi, N. T., P. N. T. Selvan, S. P. Babu, R. Pandeewari, and R. S. Daniel, "A broad-side coupled srr inspired CPW fed dual band antenna for WiMAX and wave applications," *Progress In Electromagnetics Research C*, Vol. 80, 221–231, 2018.
- [2] El Yassini, A., S. Ibnyaich, S. Chabaa, and A. Zeroual, "Miniaturized broadband-multiband planar antenna with a symmetric quarter-circular ground plane for WLAN/WiMAX standards,"

- Microwave and Optical Technology Letters*, Vol. 62, No. 9, 2953–2964, 2020.
- [3] Alam, M. M., R. Azim, N. M. Sobahi, A. I. Khan, and M. T. Islam, “A dual-band CPW-fed miniature planar antenna for S-, C-, WiMAX, WLAN, UWB, and X-band applications,” *Scientific Reports*, Vol. 12, No. 1, 7584, 2022.
- [4] Koohestani, M., N. Azadi-Tinat, and A. K. Skriversvik, “Compact slit-loaded ACS-fed monopole antenna for bluetooth and UWB systems with WLAN band-stop capability,” *IEEE Access*, Vol. 11, 7540–7550, 2023.
- [5] Naji, D. K., “A compact dual-band CPW-fed slotted-ring monopole antenna with circular fractal elements for WiMAX and C bands applications,” *Progress In Electromagnetics Research C*, Vol. 137, 123–138, 2023.
- [6] Naji, D. K., “Compact design of dual-band fractal ring antenna for WiMAX and WLAN applications,” *International Journal of Electromagnetics and Applications*, Vol. 6, No. 2, 42–50, 2016.
- [7] Mandal, T. and S. Das, “Coplanar waveguide fed 9-point star shape monopole antennas for worldwide interoperability for microwave access and wireless local area network applications,” *The Journal of Engineering*, Vol. 2014, No. 4, 155–160, 2014.
- [8] Naji, D. K., “Miniature slotted semi-circular dual-band antenna for WiMAX and WLAN applications,” *Journal of Electromagnetic Engineering and Science*, Vol. 20, No. 2, 115–124, 2020.
- [9] Ameen, M., A. Mishra, and R. K. Chaudhary, “Asymmetric CPW-fed electrically small metamaterial-inspired wideband antenna for 3.3/3.5/5.5 GHz WiMAX and 5.2/5.8 GHz WLAN applications,” *AEU — International Journal of Electronics and Communications*, Vol. 119, 153177, 2020.
- [10] Samsuzzaman, M., T. Islam, N. H. A. Rahman, M. R. I. Faruque, and J. S. Mandeep, “Coplanar waveguide fed compact wide circular-slotted antenna for Wi-Fi/WiMAX applications,” *International Journal of Antennas and Propagation*, Vol. 2014, No. 1, 982958, 2014.
- [11] Ab Rashid, A. H., B. H. Ahmad, and M. Z. A. A. Aziz, “CPW fractal antenna with third iteration of pentagonal sierpinski gasket island for 3.5 GHz WiMAX and 5.2 GHz WLAN applications,” *International Journal of Electrical and Computer Engineering Systems*, Vol. 14, No. 2, 129–134, 2023.
- [12] Naidu, V. P. and R. Kumar, “Design of compact dual-band/tri-band CPW-fed monopole antennas for WLAN/WiMAX applications,” *Wireless Personal Communications*, Vol. 82, 267–282, 2015.
- [13] Sharma, S., P. K. Singhal, and D. K. Parsediya, “A compact L-shape ACS-fed printed monopole dual-band antenna for 3.5 GHz wimax and 5.8 GHz WLAN applications,” in *Smart and Intelligent Systems*, 453–464, 2022.
- [14] Kumar, A., P. V. Naidu, M. E. Atrash, V. Kumar, and M. A. Abdalla, “A compact dual-band ACS-fed frequency independent hook loop antenna for WLAN applications,” *IETE Journal of Research*, Vol. 70, No. 5, 4523–4530, 2023.
- [15] Ansal, K. A. and T. Shanmuganatham, “Compact ACS-fed antenna with DGS and DMS for WiMAX/WLAN applications,” *International Journal of Microwave and Wireless Technologies*, Vol. 8, No. 7, 1095–1100, 2016.
- [16] Magray, M. I., K. Muzaffar, G. S. Karthikeya, and S. K. Koul, “Compact dual band F-shaped ACS-fed monopole antenna for WiMAX and WLAN applications,” in *2019 IEEE-APS Topical Conference on Antennas and Propagation in Wireless Communications (APWC)*, 126–128, Granada, Spain, 2019.
- [17] Balanis, C. A., *Antenna Theory: Analysis and Design*, John Wiley & Sons, 2016.